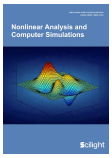
Scilight

Nonlinear Analysis and Computer Simulations
https://www.sciltp.com/journals/nacs



Article

Dynamical Control and Topological Bifurcations of Propagating Wave Patterns via Parametric Sensitivity Analysis in Nonlinear Evolution Equations

Md. Abdul Aziz [1,*] and Md. Ashik Iqbal [2]

[1] Department of Civil Engineering, Prime University, Dhaka 1216, Bangladesh
[2] Department of Applied Mathematics, University of Rajshahi, Rajshahi 6205, Bangladesh
* Correspondence: maaziz17@gmail.com

How To Cite: Aziz, M.A.; Iqbal, M.A. Dynamical Control and Topological Bifurcations of Propagating Wave Patterns via Parametric Sensitivity Analysis in Nonlinear Evolution Equations. *Nonlinear Analysis and Computer Simulations* **2026**, *1*(4), 18. https://doi.org/10.53941/nacs.2026.100018

Received: 21 August 2026
Revised: 29 September 2026
Accepted: 26 October 2026
Published: 29 October 2026

Abstract: In this research, we present a unified analytical framework for the dynamical control and topological classification of propagating wave patterns in two nonlinear evolution equations, namely the nano-ionic current (NIC) equation and the classical Sawada-Kotera (CSK) equation. We reduce two archetypal models-governing nanoscale ionic transport and dispersive wave phenomena-to planar dynamical systems by employing -expansion method. We conduct the rigorous bifurcation analysis via the discriminant of the auxiliary equation with revealing three two nondegenerate NIC configurations in which the saddle and center exchange locations between $D > 0$ and $D < 0$, together with a degenerate transition at $D = 0$. But the case the yields a degenerate rational solution, which is omitted as it does not contribute to the physically relevant wave structures. Moreover, we give a comprehensive parametric sensitivity analysis to quantify how small variations in the system parameters dynamically control the amplitude, width, and phase velocity of the resulting wave packets. We plot our obtained solutions in 3D, 2D and contour, which encompass a diverse spectrum of waveforms within their regular domains, including localized bell-shaped, kink-type, and non-compact wave profiles. The obtaining results establish that phase-plane bifurcations serve as intrinsic control knobs for tuning wave topology, offering deeper insights into wave propagation stability. For sensitivity-driven control in complex nonlinear media, this framework is not limited to specific physical models but provides a robust mathematical toolkit.

Keywords: bifurcation analysis; parametric sensitivity; dynamical control; phase-plane topology; nonlinear evolution equations; wave propagation

2020 MSC: 35C05; 35C08; 35G20

1. Introduction

In the field of nonlinear research and mathematical physics, the study of NLPDEs has proven to be a vital avenue for understanding complex wave phenomena across various scientific disciplines and in our daily lives. In fluid dynamics, turbulent flows and wave propagation are described, enabling advancements in weather prediction, oceanography, and aerodynamics. NLPDEs are fundamental in biological sciences, modeling everything from tumor growth to the spread of infectious diseases, contributing to medical breakthroughs and public health strategies. These equations are essential for understanding and developing technologies like fiber optics, semiconductors, and advanced materials in physics and engineering. Moreover, NLPDEs have found applications in social sciences and economics, helping to model human behavior, market dynamics, and decision-making

Copyright: © 2026 by the authors. This is an open access article under the terms and conditions of the Creative Commons Attribution (CC BY) license (https://creativecommons.org/licenses/by/4.0/).
Publisher's Note: Scilight stays neutral with regard to jurisdictional claims in published maps and institutional affiliations.

processes. The ubiquity of NLPDEs in describing real-world phenomena underscores their importance in advancing our understanding of nature and in developing technologies that improve human life. The NIC and CSK equations stand out as quintessential models, depicting the intricate behavior of solitary waves in various physical contexts, from fluid dynamics to plasma physics. These equations not only showcase the complex network of nonlinear interactions but also serve as a gateway to exploring the underlying mechanisms that govern wave propagation and stability. Researchers have developed and implemented a range of powerful and practical techniques for finding analytical solutions to nonlinear partial differential equations, especially, the NLPDEs. Among these approaches are: the first integral method [1], the exponential function method [2,3], the Riccati equation method [4–6], the Rieman- Hilbert method [7,8], the Jacobi elliptic function method [9,10], the Hirota's bilinear method [11,12], the tan-cot function method [13], the auxiliary equation method [14,15], the modified tanh-coth method [16], the Kudryashov method [17], the modified simple equation (MSE) method [18–20], the homogeneous balance method [21], the generalized unified method [22,23], the extended F-expansion method [24], the direct algebraic method [25,26], the Bilinear residual network method [27], the generalized Kudryashov method [28,29], the extended unified method [30,31], the Bilinear neural network method [32–34], the Backlund transform method [35], the Cole-Hopf transformation Method [36,37] etc. Li et al. introduced a notable technique called the two-variable $\left(\frac{G'}{G},\frac{1}{G}\right)$-expansion method [38]. Since that time, numerous scholars have discovered various applications for the governing progressive solitary wave solutions of NLPDEs in recent decades [39–41]. For example, a variety of new and accurate traveling wave solutions for certain NLPDEs have been obtained using the generalized $\left(\frac{G'}{G}\right)$-expansion method [42]. Recent advancements in analytical methods have opened new pathways for uncovering solutions to these challenging equations. Among these methods, the $\left(\frac{G'}{G'+G+A}\right)$-expansion technique has emerged as a powerful tool, enabling researchers to derive solitary wave solutions that exhibit remarkable properties and behaviors. Lately, several researchers have applied this method to derive analytical solutions for the integro-differential equations [43–45]. Recent studies have further demonstrated the efficiency of analytical expansion methods in obtaining exact soliton and traveling wave solutions for several important nonlinear evolution equations, including the modified Camassa-Holm, Schrödinger–Hirota, Kadomtsev-Petviashvili, and Bogoyavlensky-Konopelchenko equations [46,47]. These results reveal the flexibility and applicability of modern expansion techniques in nonlinear wave analysis. While exact solutions are valuable, understanding the parametric thresholds where waves change their shape (bifurcation) and how sensitive they are to perturbations is crucial for real-world engineering. Therefore, our paper focuses on the application of the $\left(\frac{G'}{G'+G+A}\right)$-expansion method to investigate of these problems for two significant equations: one (1 + 1) dimensional NIC equation and the CSK equation.

The CSK equation, known for its relevance in describing nonlinear wave phenomena in shallow water and ion-acoustic waves in plasmas, has been the subject of numerous studies employing various analytical methods. This equation is significant for its capacity to describe solitary wave solutions that retain their shape while traveling at a constant speed, making it applicable in fields like fluid dynamics and optical fibers. It can be effectively solved using the inverse scattering transform method, a robust approach in mathematical physics for addressing integrable equations. Its importance is highlighted by its relationships with other prominent equations in soliton theory, such as the Korteweg-de Vries equation. Additionally, the CSK equation is utilized in modeling various real-world phenomena, showcasing its versatility and relevance in scientific research [48–51]. On the other hand, the NIC equation has gained significant attention in the field of nano-biosciences, particularly in modeling ionic currents along microtubules. The study of these equations is crucial for understanding dynamical processes at the nanoscale level in biological systems. Composed of cylindrical polymers of tubulin, the is the largest components of cellular architecture, and form the structural basis of cilia and flagella, aiding in cellular and fluid movement. Their growth and shrinkage, regulated by GTP caps, are vital to their function. Understanding microtubule dynamics is important for cell biology and disease research, as well as applications in nanotechnology [52–55]. The investigation of solitary wave solutions through the expansion method provides critical insights into the behavior of NIC and CSK equations, highlighting their significance in advanced material applications. By bridging theoretical frameworks with practical implications, this research aims to contribute to the ongoing development of innovative solutions in nanotechnology and related fields. Researchers use the NIC equation to model ionic behavior at the nanoscale, which is critical for developing next-gen nanotechnologies, while they use the CSK equation to study nonlinear wave phenomena, particularly in dispersive systems like plasmas, fluids, and optical fibers. Both equations are essential in advancing the understanding of complex systems in their respective domains.

The novelty of our research could emerge from demonstrating a previously unrecognized connection or equivalence between the NIC equation and the CSK equation or other well-known integrable systems, which could broaden the applicability of your findings. If our work includes novel stability or bifurcation analysis of the

solutions, showing how small perturbations evolve, or if our asymptotic analysis provides new long-time behavior insights for these equations, that's a valuable contribution. Therefore, we can conclude that our study of solitonic solutions for the proposed equations can offer valuable insights into wave propagation, quantum mechanics, and nanoscale systems. The NIC equation describes the dynamics of ionic currents at the nanoscale, which plays a crucial role in advanced nanotechnology devices, including nano-sensors and energy storage devices. On the other hand, the CSK equation is a fifth-order nonlinear equation that appears in fluid dynamics, plasma physics, and optical systems. It generalizes various existing methods and provides a systematic way to derive solitonic solutions. In this paper, we apply $\left(\frac{G'}{G'+G+A}\right)$- expansion method to both the NIC equation and the CSK equation, aiming to find novel solitonic solutions that can deepen our understanding of their behaviors.

In this research, our aim to bridge the gap between purely analytical soliton solutions and dynamical systems theory. Two distinct nonlinear evolution models have been investigated to demonstrate a universal protocol: (i) derive traveling wave reduction, (ii) extract exact solutions, (iii) reconstruct the planar dynamical system, (iv) classify topological bifurcations, and (v) perform sensitivity analysis. This approach transforms the conventional solve-and-plot routine into a predictive dynamical control framework.

Therefore, we make the paper as follows: In Section 2, the methodology is given. Applications of the suggested method have been explored through the expansion method in Sections 3 and 4. Planar dynamical system, bifurcation topology, and parametric sensitivity are given in Section 5. We give the 3D, 2D and contour figures of the solutions and analysis in Section 6. We compare our results and mention the originality of our findings in Section 7, and finally, we give the conclusions in Section 8.

2. A Short Note of the Proposed Method

In this part, we outline our systematic approach to identifying the most effective solutions for NLPDEs. By utilizing advanced problem-solving techniques, we aim to develop innovative methodologies that enhance the accuracy and efficiency of solutions. Let us consider a particular NLPDE as below,

$$(v, v_x, v_t, v_{xx}, v_{xt}, v_{tt}, \dots) = 0. \tag{1}$$

where, P is an algebraic expression of $v, v_x, v_t, v_{xx}, v_{xt}, v_{tt}, \dots$ and it involves partial derivatives. The essential actions are summarized below:

Action I: In the beginning, we must transform the given partial differential equation into the form of an ordinary differential equation (ODE). By implementing the wave transformation principles, the ODE results of Equation (1) can be written as follows:

$$v(x,\ t) = v(\omega), \tag{2}$$

where $\omega = x - ct$, such that c is the wave velocity.

By differentiating Equation (2) multiple times as required, we get the ordinary differential equation of Equation (1),

$$Q(v,\ v',\ v'',\ v'',\ \dots) = 0. \tag{3}$$

Here, the primes indicate the ordinary derivatives with respect to ω.

Action II: Say, the solution of Equation (3) as follows,

$$v(\omega) = \sum_{l=0}^{M} a_l \left(\frac{G'}{G'+G+A}\right)^l, \tag{4}$$

where M is the polynomial's degree, and $G(\omega)$ represents the following ODE:

$$G'' + SG' + TG + TA = 0. \tag{5}$$

Now, from the proposed method, we have to find out the values of constant terms $A, S, T,$ and a_l $(l = 0, 1, 2, \dots M)$. By the homogeneous balance rule in Equation (3), we get the values of M and put it in Equation (4). For getting a set of algebraic equations, we need the derivative with respect to ω then put in Equation (3). By analyzing the system of equations, we can determine the values of a_l $(l = 0, 1, 2, \dots M)$ then allow us to derive the function $G(\omega)$ by using Equation (5).

Action III: Finally, from Equations (3) and (4), we get an algebraic expression of $\left(\frac{G'}{G'+G+A}\right)$ in terms of $S, T,$ and a_l. Consequently, the collection of coefficients is set to zero. After some operations, we determine the discriminant from the auxiliary Equation (5), and we will obtain the solutions in the form of trigonometric and

exponential functions. Now, we insert the values of G into the polynomial $\left(\frac{G'}{G'+G+A}\right)$, and we can arrive at the final result of Equation (1).

Action IV: In action III, i.e., Equation (3), the reduced ODE obtained constitutes the core mathematical foundation for our dynamical analysis. We reinterpret it as a planar dynamical system by introducing the transformation $v' = y$ and $v'' = y'$ rather than treating it merely as an algebraic equation for deriving exact solutions, which allows us to map the wave propagation problem onto a phase-plane, where the equilibrium points and their stability characteristics are determined by the system parameters. Whether the topological nature of the trajectories form open orbits, closed cycles, or homoclinic loops is directly governed by the discriminant of the auxiliary equation, thereby establishing a direct link between the algebraic soliton solutions and the underlying dynamical behavior. As a result, the reduced ODE in Equation 3 will be treated as a planar dynamical system to explore its phase-plane topology and bifurcation thresholds.

3. Applications of the Expansion Method to the NIC Equation

In this segment, we explore the factors and conditions that allow microtubules to function as nonlinear electrical conduits for ion movement along their cylindrical structures. It has led to the development of a model where individual tubulin dimer proteins serve as electrical components [56]. The following mathematical model equation, namely, the NIC equation is designed to compute the behavior of nano-ionic currents along microtubules,

$$\frac{hn_0}{m}u_t + 2u_x - \frac{h^{3/2}n_0}{m}\left(2\rho - \varphi\frac{G_0}{n_0}\right)uu_t + \frac{m^2}{3}u_{xxx} + \left(\frac{rh^{-1}-G_0h}{m}\right)u = 0. \tag{6}$$

We apply $rh^{-1} - G_0h = 0$, because of ohmic loss and we find the exact wave solutions of Equation (6) is as follows:

$$\frac{hn_0}{m}u_t + 2u_x - \frac{h^{3/2}n_0}{m}\left(2\rho - \varphi\frac{G_0}{n_0}\right)uu_t + \frac{m^2}{3}u_{xxx} = 0. \tag{7}$$

The symbols indicate the following: h be the characteristic impedance, the total maximum capacitance as n_0, m be the length, ρ is the nonlinearity of the conductance of nano-pores, the capacitor as φ, *r* is the leading elementary capacitor and the conductance of pertaining nano-pores as G_0 [56]. Let us consider the wave transformations, we use $u(x,t) = u(\delta);\ \delta = \frac{1}{m}x - \frac{\varepsilon}{\tau}t$ in Equation (7), and get the following ODE form,

The traveling coordinate can be written in the following equivalent form, which gives the physical NIC wave speed used throughout the revised discussion:

$$\delta = \frac{x}{m} - \frac{\varepsilon t}{\tau} = \frac{1}{m}(x - c_{\text{NIC}}t).$$

$$c_{\text{NIC}} = \frac{m\varepsilon}{\tau}.$$

$$u''' - \beta\varepsilon uu' + (6 - \gamma\varepsilon)u' = 0, \tag{8}$$

where prime denotes the derivatives of u with respect to δ, and $\beta = \frac{3h^{3/2}n_0}{\tau}\left(\varphi\frac{G_0}{n_0} - 2\rho\right)$, $\gamma = \frac{3hn_0}{\tau}$.

Integrating Equation (8) once gives the following first integral:

The first integration is written with its integration constant as

$$u'' - \frac{\beta\varepsilon}{2}u^2 + (6 - \gamma\varepsilon)u = C_{\text{NIC}}.$$

For the localized zero-background traveling-wave class considered here, the following asymptotic conditions are imposed:

$$u(\delta) \to 0, \qquad u'(\delta) \to 0, \qquad u''(\delta) \to 0 \quad \text{as} \quad |\delta| \to \infty.$$

Now, $C_{\text{NIC}} = 0$ implies,

$$u'' - \beta\varepsilon\frac{u^2}{2} + (6 - \gamma\varepsilon)u = 0 \tag{9}$$

We apply the balancing formula u'' with u^2 in Equation (9), and get the $M = 2$. Now, we can write Equation (4) as follows:

$$u(\omega) = a_0 + a_1\left(\frac{G'}{G'+G+A}\right) + a_2\left(\frac{G'}{G'+G+A}\right)^2. \tag{10}$$

Here, the arbitrary constants a_0, a_1, and a_2 must be calculated.

For the constant values a_0, a_1, and a_2, using computer programs to the Equations (9) and (10) yields two sets of algebraic equations as follows:

Set 1: $a_0 = a_0,\ a_1 = \frac{a_0(S-2T)}{T},\ a_2 = -\frac{a_0(S-T-1)}{T},\ \beta = -\frac{12(S-T-1)T}{\varepsilon a_0},\ \gamma = \frac{S^2-4T+6}{\varepsilon},\ \varepsilon = \varepsilon.$

Set 2: $a_0 = a_0,\ a_1 = -\frac{6a_0(S^2-3ST-S+2T^2+2T)}{S^2+2T-6ST+6T^2}, a_2 = \frac{6a_0(1-2S+T^2+2T-2ST+S^2)}{S^2+2T-6ST+6T^2},\ \beta = \frac{2(S^2+2T-6ST+6T^2)}{\varepsilon a_0},\ \gamma = -\frac{S^2-4T-6}{\varepsilon},\ \varepsilon = \varepsilon.$

By inserting the values of the constants from set 1 into Equation (10), two scenarios arise that give the actual results for Equation (6).

Scenario I: For $D = S^2 - 4T > 0$,

$$u(\delta) = a_0 + \left[\frac{a_0(S-2T)}{T}\right] \times \left[\frac{A_1(S+\sqrt{D})+A_2(S-\sqrt{D})e^{\sqrt{D}\delta}}{A_1(S+\sqrt{D}-2)+A_2(S-\sqrt{D}-2)e^{\sqrt{D}\delta}}\right] - \left[\frac{a_0(S-T-1)}{T}\right] \times \left[\frac{A_1(S+\sqrt{D})+A_2(S-\sqrt{D})e^{\sqrt{D}\delta}}{A_1(S+\sqrt{D}-2)+A_2(S-\sqrt{D}-2)e^{\sqrt{D}\delta}}\right]^2, \tag{11}$$

where, A_1 and A_2 are constants. For the final solution of Equation (6), setting $\delta = \frac{1}{m}x - \frac{\varepsilon}{\tau}t$ in Equation (11),

$$u(x,t) = a_0 + \left[\frac{a_0(S-2T)}{T}\right] \times \left[\frac{A_1(S+\sqrt{D})+A_2(S-\sqrt{D})e^{\sqrt{D}\left(\frac{1}{m}x-\frac{\varepsilon}{\tau}t\right)}}{A_1(S+\sqrt{D}-2)+A_2(S-\sqrt{D}-2)e^{\sqrt{D}\left(\frac{1}{m}x-\frac{\varepsilon}{\tau}t\right)}}\right] - \left[\frac{a_0(S-T-1)}{T}\right] \times \left[\frac{A_1(S+\sqrt{D})+A_2(S-\sqrt{D})e^{\sqrt{D}\left(\frac{1}{m}x-\frac{\varepsilon}{\tau}t\right)}}{A_1(S+\sqrt{D}-2)+A_2(S-\sqrt{D}-2)e^{\sqrt{D}\left(\frac{1}{m}x-\frac{\varepsilon}{\tau}t\right)}}\right]^2. \tag{12}$$

Scenario II: For $D = S^2 - 4T < 0$,

$$u(\delta) = a_0 + \left[\frac{a_0(S-2T)}{T}\right] \times \left[\frac{(SA_2+A_1\sqrt{-D})\sin\left(\frac{\sqrt{-D}}{2}\delta\right)+(SA_1-A_2\sqrt{-D})cos\left(\frac{\sqrt{-D}}{2}\delta\right)}{((S-2)A_2+A_1\sqrt{-D})\sin\left(\frac{\sqrt{-D}}{2}\delta\right)+((S-2)A_1+A_2\sqrt{-D})cos\left(\frac{\sqrt{-D}}{2}\delta\right)}\right] - \left[\frac{a_0(S-T-1)}{T}\right] \times \left[\frac{(SA_2+A_1\sqrt{-D})\sin\left(\frac{\sqrt{-D}}{2}\delta\right)+(SA_1-A_2\sqrt{-D})cos\left(\frac{\sqrt{-D}}{2}\delta\right)}{((S-2)A_2+A_1\sqrt{-D})\sin\left(\frac{\sqrt{-D}}{2}\delta\right)+((S-2)A_1+A_2\sqrt{-D})cos\left(\frac{\sqrt{-D}}{2}\delta\right)}\right]^2. \tag{13}$$

For the final result of Equation (6), putting $\delta = \frac{1}{m}x - \frac{\varepsilon}{\tau}t$ in Equation (13),

$$\boldsymbol{u(x,t) = a_0 + \left[\frac{a_0(S-2T)}{T}\right] \times}$$

$$\left[\frac{(SA_2+A_1\sqrt{-D})\sin\left(\frac{\sqrt{-D}}{2}\left[\frac{1}{m}x-\frac{\varepsilon}{\tau}t\right]\right)+(SA_1-A_2\sqrt{-D})cos\left(\frac{\sqrt{-D}}{2}\left[\frac{1}{m}x-\frac{\varepsilon}{\tau}t\right]\right)}{((S-2)A_2+A_1\sqrt{-D})\sin\left(\frac{\sqrt{-D}}{2}\left[\frac{1}{m}x-\frac{\varepsilon}{\tau}t\right]\right)+((S-2)A_1+A_2\sqrt{-D})cos\left(\frac{\sqrt{-D}}{2}\left[\frac{1}{m}x-\frac{\varepsilon}{\tau}t\right]\right)}\right] - \left[\frac{a_0(S-T-1)}{T}\right] \times \left[\frac{(SA_2+A_1\sqrt{-D})\sin\left(\frac{\sqrt{-D}}{2}\left[\frac{1}{m}x-\frac{\varepsilon}{\tau}t\right]\right)+(SA_1-A_2\sqrt{-D})cos\left(\frac{\sqrt{-D}}{2}\left[\frac{1}{m}x-\frac{\varepsilon}{\tau}t\right]\right)}{((S-2)A_2+A_1\sqrt{-D})\sin\left(\frac{\sqrt{-D}}{2}\left[\frac{1}{m}x-\frac{\varepsilon}{\tau}t\right]\right)+((S-2)A_1+A_2\sqrt{-D})cos\left(\frac{\sqrt{-D}}{2}\left[\frac{1}{m}x-\frac{\varepsilon}{\tau}t\right]\right)}\right]^2. \tag{14}$$

Regularity qualification for Equations (13), (14), (17) and (18): Let $\omega = \sqrt{(-D)}/2$ and define $B = (S-2)A^2 + A^1\sqrt{-D},\ C = (S-2)A_1 + A_2\sqrt{(-D)}$. The shared trigonometric denominator is $B\,sin(\omega\delta) + C\,cos(\omega\delta)$. If $D < 0$ and $(B,C) \neq (0,0)$, it vanishes at infinitely many real δ; accordingly these formulae are meromorphic and cannot be described as globally nonsingular. Their plots must avoid poles. If $B = C = 0$, the given expressions are undefined.

Again, setting the values of the constants from set 2 into Equation (10) and two scenarios arise that give the actual results for Equation (6).

Scenario I: For $D = S^2 - 4T > 0$,

$$u(\delta) = a_0 - \left[\frac{6a_0(S^2-3ST-S+2T^2+2T)}{S^2+2T-6ST+6T^2}\right] \times \left[\frac{A_1(S+\sqrt{D})+A_2(S-\sqrt{D})e^{\sqrt{D}\delta}}{A_1(S+\sqrt{D}-2)+A_2(S-\sqrt{D}-2)e^{\sqrt{D}\delta}}\right] + \left[\frac{6a_0(1-2S+T^2+2T-2ST+S^2)}{S^2+2T-6ST+6T^2}\right] \times \left[\frac{A_1(S+\sqrt{D})+A_2(S-\sqrt{D})e^{\sqrt{D}\delta}}{A_1(S+\sqrt{D}-2)+A_2(S-\sqrt{D}-2)e^{\sqrt{D}\delta}}\right]^2 \tag{15}$$

where A_1 and A_2 are constants. For the final solution of Equation (6), setting $\delta = \frac{1}{m}x - \frac{\varepsilon}{\tau}t$ in Equation (15),

$$u(x,t) = a_0 - \left[\frac{6a_0(S^2-3ST-S+2T^2+2T)}{S^2+2T-6ST+6T^2}\right] \times \left[\frac{A_1(S+\sqrt{D})+A_2(S-\sqrt{D})e^{\sqrt{D}\left(\frac{1}{m}x-\frac{\varepsilon}{\tau}t\right)}}{A_1(S+\sqrt{D}-2)+A_2(S-\sqrt{D}-2)e^{\sqrt{D}\left(\frac{1}{m}x-\frac{\varepsilon}{\tau}t\right)}}\right] + \left[\frac{6a_0(1-2S+T^2+2T-2ST+S^2)}{S^2+2T-6ST+6T^2}\right] \times \left[\frac{A_1(S+\sqrt{D})+A_2(S-\sqrt{D})e^{\sqrt{D}\left(\frac{1}{m}x-\frac{\varepsilon}{\tau}t\right)}}{A_1(S+\sqrt{D}-2)+A_2(S-\sqrt{D}-2)e^{\sqrt{D}\left(\frac{1}{m}x-\frac{\varepsilon}{\tau}t\right)}}\right]^2 \tag{16}$$

Scenario II: For $D = S^2 - 4T < 0$,

$$u(\delta) = a_0 - \left[\frac{6a_0(S^2-3ST-S+2T^2+2T)}{S^2+2T-6ST+6T^2}\right] \times \left[\frac{(SA_2+A_1\sqrt{-D})\sin\left(\frac{\sqrt{-D}}{2}\delta\right)+(SA_1-A_2\sqrt{-D})cos\left(\frac{\sqrt{-D}}{2}\delta\right)}{\left((S-2)A_2+A_1\sqrt{-D}\right)\sin\left(\frac{\sqrt{-D}}{2}\delta\right)+\left((S-2)A_1+A_2\sqrt{-D}\right)cos\left(\frac{\sqrt{-D}}{2}\delta\right)}\right] + \left[\frac{6a_0(1-2S+T^2+2T-2ST+S^2)}{S^2+2T-6ST+6T^2}\right] \times \left[\frac{(SA_2+A_1\sqrt{-D})\sin\left(\frac{\sqrt{-D}}{2}\delta\right)+(SA_1-A_2\sqrt{-D})cos\left(\frac{\sqrt{-D}}{2}\delta\right)}{\left((S-2)A_2+A_1\sqrt{-D}\right)\sin\left(\frac{\sqrt{-D}}{2}\delta\right)+\left((S-2)A_1+A_2\sqrt{-D}\right)cos\left(\frac{\sqrt{-D}}{2}\delta\right)}\right]^2 \tag{17}$$

For the final result of Equation (6), putting $\delta = \frac{1}{m}x - \frac{\varepsilon}{\tau}t$ in Equation (17),

$$\boldsymbol{u(x,t) = a_0 - \left[\frac{6a_0(S^2-3ST-S+2T^2+2T)}{S^2+2T-6ST+6T^2}\right] \times \left[\frac{(SA_2+A_1\sqrt{-D})\sin\left(\frac{\sqrt{-D}}{2}\left[\frac{1}{m}x-\frac{\varepsilon}{\tau}t\right]\right)+(SA_1-A_2\sqrt{-D})cos\left(\frac{\sqrt{-D}}{2}\left[\frac{1}{m}x-\frac{\varepsilon}{\tau}t\right]\right)}{\left((S-2)A_2+A_1\sqrt{-D}\right)\sin\left(\frac{\sqrt{-D}}{2}\left[\frac{1}{m}x-\frac{\varepsilon}{\tau}t\right]\right)+\left((S-2)A_1+A_2\sqrt{-D}\right)cos\left(\frac{\sqrt{-D}}{2}\left[\frac{1}{m}x-\frac{\varepsilon}{\tau}t\right]\right)}\right] + \left[\frac{6a_0(1-2S+T^2+2T-2ST+S^2)}{S^2+2T-6ST+6T^2}\right] \times \left[\frac{(SA_2+A_1\sqrt{-D})\sin\left(\frac{\sqrt{-D}}{2}\left[\frac{1}{m}x-\frac{\varepsilon}{\tau}t\right]\right)+(SA_1-A_2\sqrt{-D})cos\left(\frac{\sqrt{-D}}{2}\left[\frac{1}{m}x-\frac{\varepsilon}{\tau}t\right]\right)}{\left((S-2)A_2+A_1\sqrt{-D}\right)\sin\left(\frac{\sqrt{-D}}{2}\left[\frac{1}{m}x-\frac{\varepsilon}{\tau}t\right]\right)+\left((S-2)A_1+A_2\sqrt{-D}\right)cos\left(\frac{\sqrt{-D}}{2}\left[\frac{1}{m}x-\frac{\varepsilon}{\tau}t\right]\right)}\right]^2} \tag{18}$$

4. Applications of the Expansion Method to the CSK Equation

The CSK equation, first introduced by Sawada and Kotera in 1974, emerged as a significant contribution to the study of nonlinear waves, particularly in the context of soliton theory [51]. This integrable partial differential equation is notable for its ability to describe the dynamics of solitons, stable waveforms that maintain their shape while traveling at constant speeds. Its utility in modeling phenomena such as rogue waves and pulse propagation in optical fibers has made it an essential tool for researchers exploring nonlinear effects in various media [57,58]. In many fields of applied science and engineering, the significance of analytical solutions is growing, as the enhancement of our comprehension of nonlinear processes and their possible practical applications. Furthermore, investigating traveling wave structures is essential for accurately understanding and implementing these wave phenomena. Sawada and Kotera presented the classical (1 + 1)-dimensional equation, highlighting the presence of multiple solutions [49] and the nonlinear model equation is given by:

$$\partial v/\partial t + \partial^5 v/\partial x^5 + 15v\partial^3 v/\partial x^3 + 15(\partial v/\partial x)(\partial^2 v/\partial x^2) + 45v^2\partial v/\partial x = 0 \tag{19}$$

We convert the Equation (19) into ODE format through the transformation, $v(x,t) = u(\delta);\ \delta = x - ct$, we get,

$$-cv' + 45v^2v' + 15v'v'' + 15vv''' + v''''' = 0. \tag{20}$$

Sign convention: Equation (19) is written with $+15vv_{xxx} + 15v_xv_{xx}$, which yields the positive nonlinear derivative terms in Equation (20) under $\delta = x - ct$. The alternative negative-sign model is not being analyzed here. For Set 1, differentiation of $v = b + 2k^2$ sech^2(kδ) verifies Equation (20) when $c = 45b^2 + 60bk^2 + 16k^4$.

Integrating Equation (20) the CSK traveling-wave equation once gives

$$v^{(4)} + 15vv'' + 15v^3 - cv = C_{\mathrm{CSK}}.$$

For zero-background localized profiles (b = 0), the integration constant vanishes; nonzero-background Set-1 solutions retain the appropriate nonzero integration constant. The homogeneous balance is then performed between the fourth-derivative term and the cubic term. The same expansion order is obtained directly from the unintegrated equation:

$$C_{\mathrm{CSK}} = 0.$$

$$M + 4 = 3M,$$

$$M = 2,$$

$$M + 5 = 3M + 1,$$

$$M = 2.$$

Therefore, Equation (21) is taken with $M = 2$.

$$v(\omega) = a_0 + a_1\left(\frac{G'}{G'+G+A}\right) + a_2\left(\frac{G'}{G'+G+A}\right)^2. \tag{21}$$

Here, the arbitrary constants a_0, a_1 and a_2 must be found out.

For the constant values a_0, a_1, and a_2, using computer programs to the Equations (20) and (21) gives two sets of algebraic equations as follows:

Set 1: (verified family): $v(\delta) = b + 2k^2\,\mathrm{sech}^2(k\delta)$, $k \neq 0$, with $c = 45b^2 + 60bk^2 + 16k^4$. Direct substitution into Equation (20) yields zero residual. The earlier polynomial Set-1 coefficients and the corresponding expressions previously printed as Equations (22)–(25) are replaced by the following equivalent representatives of this verified family.

Set 2: $a_0 = -\frac{S^2}{3} + 4ST - 4T^2 - \frac{8T}{3}$, $a_1 = 4S^2 + 8T^2 + 8T - 4S - 12ST$, $a_2 = -4 + 8S - 4S^2 - 8T + 8ST - 4T^2$, $c = S^4 - 8S^2T + 16T^2$.

The Set-1 representative solutions for the CSK equation are as follows:

Scenario I: Centered localized solution:

$$v(\delta) = a_0 + [2S^2 + 4T^2 + 4T - 2S - 6ST] \times \left[\frac{A_1(S+\sqrt{D}) + A_2(S-\sqrt{D})e^{\sqrt{D}\delta}}{A_1(S+\sqrt{D}-2) + A_2(S-\sqrt{D}-2)e^{\sqrt{D}\delta}}\right] + v(\delta) = b + 2k^2\,\mathrm{sech}^2(k\delta),\ k \neq 0 \tag{22}$$

Substituting $\delta = x - ct$, where $c = 45b^2 + 60bk^2 + 16k^4$, gives

$$v(x,t) = a_0 + [2S^2 + 4T^2 + 4T - 2S - 6ST] \times \left[\frac{A_1(S+\sqrt{D}) + A_2(S-\sqrt{D})e^{\sqrt{D}(x-ct)}}{A_1(S+\sqrt{D}-2) + A_2(S-\sqrt{D}-2)e^{\sqrt{D}(x-ct)}}\right] + v(x,t) = b + 2k^2\,\mathrm{sech}^2[k(x - ct)] \tag{23}$$

Scenario II: Spatially translated member of the same exact family:

$$v(\delta) = b + 2k^2\,\mathrm{sech}^2[k(\delta - \delta_0)] \tag{24}$$

Substitution of $\delta = x - ct$ yields

$$v(x,t) = a_0 + [2S^2 + 4T^2 + 4T - 2S - 6ST] \times v(x,t) = b + 2k^2\mathrm{sech}^2[k(x - ct - \delta_0)] \tag{25}$$

Again, setting the constants values from set 2 into Equation (21) and two scenarios arise that give the actual results for Equation (19).

Scenario I: For $D = S^2 - 4T > 0$,

$$v(\delta) = \left[-\frac{S^2}{3} + 4ST - 4T^2 - \frac{8T}{3}\right] + [4S^2 + 8T^2 + 8T - 4S - 12ST] \times \left[\frac{A_1(S+\sqrt{D}) + A_2(S-\sqrt{D})e^{\sqrt{D}\delta}}{A_1(S+\sqrt{D}-2) + A_2(S-\sqrt{D}-2)e^{\sqrt{D}\delta}}\right] + [-4 + 8S - 4S^2 - 8T + 8ST - 4T^2] \times \left[\frac{A_1(S+\sqrt{D}) + A_2(S-\sqrt{D})e^{\sqrt{D}\delta}}{A_1(S+\sqrt{D}-2) + A_2(S-\sqrt{D}-2)e^{\sqrt{D}\delta}}\right]^2 \tag{26}$$

By setting $\delta = x - ct$ in Equation (26),

$$v(x,t) = \left[-\frac{S^2}{3} + 4ST - 4T^2 - \frac{8T}{3}\right] + [4S^2 + 8T^2 + 8T - 4S - 12ST] \times \left[\frac{A_1(S+\sqrt{D}) + A_2(S-\sqrt{D})e^{\sqrt{D}(x-ct)}}{A_1(S+\sqrt{D}-2) + A_2(S-\sqrt{D}-2)e^{\sqrt{D}(x-ct)}}\right] + [-4 + 8S - 4S^2 - 8T + 8ST - 4T^2] \times \left[\frac{A_1(S+\sqrt{D}) + A_2(S-\sqrt{D})e^{\sqrt{D}(x-ct)}}{A_1(S+\sqrt{D}-2) + A_2(S-\sqrt{D}-2)e^{\sqrt{D}(x-ct)}}\right]^2 \tag{27}$$

Scenario II: For $D = S^2 - 4T < 0$,

$$v(\delta) = \left[-\frac{S^2}{3} + 4ST - 4T^2 - \frac{8T}{3}\right] + [4S^2 + 8T^2 + 8T - 4S - 12ST] \times \left[\frac{(SA_2 + A_1\sqrt{-D})\sin\left(\frac{\sqrt{-D}}{2}\delta\right) + (SA_1 - A_2\sqrt{-D})cos\left(\frac{\sqrt{-D}}{2}\delta\right)}{((S-2)A_2 + A_1\sqrt{-D})\sin\left(\frac{\sqrt{-D}}{2}\delta\right) + ((S-2)A_1 + A_2\sqrt{-D})cos\left(\frac{\sqrt{-D}}{2}\delta\right)}\right] + [-4 + 8S - 4S^2 - 8T + 8ST - 4T^2] \times \left[\frac{(SA_2 + A_1\sqrt{-D})\sin\left(\frac{\sqrt{-D}}{2}\delta\right) + (SA_1 - A_2\sqrt{-D})cos\left(\frac{\sqrt{-D}}{2}\delta\right)}{((S-2)A_2 + A_1\sqrt{-D})\sin\left(\frac{\sqrt{-D}}{2}\delta\right) + ((S-2)A_1 + A_2\sqrt{-D})cos\left(\frac{\sqrt{-D}}{2}\delta\right)}\right]^2 \quad (28)$$

Using $\delta = x - ct$ in Equation (28),

$$v(x,t) = \left[-\frac{S^2}{3} + 4ST - 4T^2 - \frac{8T}{3}\right] + [4S^2 + 8T^2 + 8T - 4S - 12ST] \times \left[\frac{(SA_2 + A_1\sqrt{-D})\sin\left(\frac{\sqrt{-D}}{2}[x-ct]\right) + (SA_1 - A_2\sqrt{-D})cos\left(\frac{\sqrt{-D}}{2}[x-ct]\right)}{((S-2)A_2 + A_1\sqrt{-D})\sin\left(\frac{\sqrt{-D}}{2}[x-ct]\right) + ((S-2)A_1 + A_2\sqrt{-D})cos\left(\frac{\sqrt{-D}}{2}[x-ct]\right)}\right] + [-4 + 8S - 4S^2 - 8T + 8ST - 4T^2] \times \left[\frac{(SA_2 + A_1\sqrt{-D})\sin\left(\frac{\sqrt{-D}}{2}[x-ct]\right) + (SA_1 - A_2\sqrt{-D})cos\left(\frac{\sqrt{-D}}{2}[x-ct]\right)}{((S-2)A_2 + A_1\sqrt{-D})\sin\left(\frac{\sqrt{-D}}{2}[x-ct]\right) + ((S-2)A_1 + A_2\sqrt{-D})cos\left(\frac{\sqrt{-D}}{2}[x-ct]\right)}\right]^2 \quad (29)$$

The two arbitrary constants arise from the general auxiliary solution. A common nonzero rescaling cancels in the ratio used by the expansion ansatz; therefore, only their ratio is essential. For the exponential branch the ratio primarily produces a translation, while for trigonometric branches it produces a phase shift. This is expressed by the constants below:

$$A_1,\ A_2.$$

5. Planar Dynamical System, Bifurcation Topology, and Parametric Sensitivity

In this part, we reinterpret the reduced ODEs obtained from the NIC and CSK models as planar dynamical systems, which allows us to classify the topological bifurcations and to quantify how parameter variations dynamically control the propagating wave patterns.

5.1. Bifurcation Analysis for the NIC Model

For the NIC equation in Equation (9), let the discriminant of the auxiliary equation be

$$D = S^2 - 4T.$$

Without introducing any additional coefficient notation, the reduced NIC equation can be written directly as

$$u'' = Du - \frac{6(S - T - 1)T}{a_0} u^2.$$

The following nondegeneracy conditions are required for the second equilibrium to be well defined:

$$T \neq 0,\ \ a_0 \neq 0,\ \ S - T - 1 \neq 0.$$

Introducing the phase variable $y = u'$ gives the planar system

$$u' = y,\ \ y' = Du - \frac{6(S - T - 1)T}{a_0} u^2.$$

The equilibrium points are

$$E_1 = (0,0), E_2 = \left(\frac{a_0 D}{6(S - T - 1)T}, 0\right).$$

The Jacobian has zero trace, and its determinants at the equilibria are

$$det\, J(E_1) = -D,\ \ det\, J(E_2) = D.$$

Hence, for $D > 0$, E_1 is a saddle and E_2 is a center; for $D < 0$, E_1 is a center and E_2 is a saddle. The nonlinear center classification is not inferred from the Jacobian alone. Multiplying the reduced equation by u' and integrating yields the first integral

$$H(u,y) = \frac{1}{2}y^2 - \frac{1}{2}Du^2 + \frac{2(S - T - 1)T}{a_0}u^3 = C.$$

At the equilibrium classified as a center, the effective potential has a strict local minimum; therefore, nearby regular level sets of H are closed. The separatrix and open trajectories are determined by the corresponding energy levels. This first-integral argument provides the nonlinear phase-plane justification requested by the reviewer.

At the transition value $D = 0$, the two equilibria coalesce and the linearization becomes non-hyperbolic. We therefore describe $D = 0$ as a degenerate bifurcation threshold rather than identifying it as a homoclinic boundary without an additional global-orbit argument. The equilibrium classification and corresponding wave-profile implications for different values of (D) are summarized in Table 1.

Table 1. Equilibrium classification and wave-profile implications.

Condition	Correct Dynamical Interpretation	Wave-Profile Implication
$D > 0$ ($K \neq 0$)	E_1 saddle; E_2 nonlinear center. Closed levels occur near E_2; separatrix/open levels follow from H.	Profile type must be determined from the explicit solution and its asymptotic limits.
$D < 0$ ($K \neq 0$)	E_1 nonlinear center; E_2 saddle. Roles are exchanged relative to $D > 0$.	Nonsingular trigonometric branches are periodic/oscillatory; compact support is not implied.
$D = 0$	Coalesced non-hyperbolic equilibrium (degenerate transition).	No homoclinic claim is made without a separate global analysis.

5.2. Bifurcation Analysis for the CSK Model

For the verified CSK Set-1 family in Equations (22)–(25), let $w(\delta) = v(\delta) - b = 2k^2\,\mathrm{sech}^2[k(\delta - \delta_0)]$, with $k \neq 0$. The following second-order equation is an identity for this exact family, not an equivalent reduction of the full fifth-order CSK equation.

Define the translated profile and its derivative:

$$w(\delta) = 2k^2\,\mathrm{sech}^2[k(\delta - \delta_0)], \quad z = w'(\delta).$$

Differentiation gives

$$w' = -4k^3\,\mathrm{sech}^2[k(\delta - \delta_0)]\,tanh[k(\delta - \delta_0)].$$

The resulting second-order equation is

$$w'' = 4k^2w - 3w^2.$$

Accordingly, the corresponding planar system is

$$w' = z, \quad z' = 4k^2w - 3w^2.$$

The equilibrium states and Jacobian determinants are

$$(w, z) = (0,0), (4k^2/3,0); \quad det\,J(0,0) = -4k^2, \; det\,J(4k^2/3,0) = 4k^2.$$

Thus, the first equilibrium is a saddle and the second is a center for real $k \neq 0$. This classification is specific to the verified pulse family.

Multiplying the second-order relation by w' gives the conserved quantity

$$H(w, z) = ½z^2 - 2k^2w^2 + w^3 = constant.$$

The zero-energy level contains the localized homoclinic pulse associated with the saddle $w = 0$.

Direct symbolic differentiation verifies that the same profile, with wave speed $c = 45b^2 + 60bk^2 + 16k^4$, satisfies the fifth-order traveling-wave Equation (20).

The result does not establish the topology of the entire fifth-order CSK solution space or a $D < 0$ branch of the CSK Set-1 family.

The auxiliary discriminant $D = S^2 - 4T$ remains relevant to the NIC auxiliary construction, but is not identified here with $4k^2$ unless a parameterization is explicitly imposed.

Therefore, the earlier claim of an identical D-dependent saddle/center exchange for the two complete models is not made.

For this selected pulse, the second-order relation is

$$w'' - 4k^2w + 3w^2 = 0.$$

The normal-form coefficients and their parameter restrictions are

$$\alpha = -4k^2, \quad \beta = 3, \quad k \in \mathbb{R}\backslash\{0\}.$$

The first integral remains valid for real $k \neq 0$.

$$H(w,z) = \tfrac{1}{2}z^2 - 2k^2w^2 + w^3.$$

The Set-1 family thus has the stated saddle–center phase portrait; no unverified equivalence with the $D < 0$ NIC family is asserted.

5.3. Parametric Sensitivity Analysis

For the nonsingular positive-discriminant Set-1 pulse, a convenient translated representative is

$$u(\delta) = \frac{a_0 D}{4kT}\operatorname{sech}^2\left[\frac{\sqrt{D}}{2}(\delta - \delta_0)\right], \qquad D > 0.$$

The representative pulse is

$$u(\delta) = \frac{a_0 D}{4kT}\operatorname{sech}^2\left[\frac{\sqrt{D}}{2}(\delta - \delta_0)\right], \qquad D > 0.$$

The peak amplitude and the full width at half maximum are defined by

$$A(S) = \left|\frac{a_0 D}{4kT}\right|,$$

$$W_{\mathrm{FWHM}}(S) = \frac{4\operatorname{arcosh}(\sqrt{2})}{\sqrt{D}}.$$

The corresponding quantities are

$$A(S) = \left|\frac{a_0 D}{4kT}\right|,$$

$$W_{\mathrm{FWHM}}(S) = \frac{4\operatorname{arcosh}(\sqrt{2})}{\sqrt{D}}.$$

The sensitivities are the derivatives of these quantities with respect to the control parameter. For the illustrative fixed-parameter choice and the positive branch, the admissible conditions are

$$\frac{dA}{dS}, \qquad \frac{dW_{\mathrm{FWHM}}}{dS}.$$

$$T = 1, \qquad a_0 > 0, \qquad S > 2.$$

For this illustrative choice, the amplitude and its sensitivity reduce to

$$A(S) = \frac{a_0(S+2)}{4}, \qquad \frac{dA}{dS} = \frac{a_0}{4}.$$

The width and its sensitivity reduce to

$$W_{\mathrm{FWHM}}(S) = \frac{4\operatorname{arcosh}(\sqrt{2})}{\sqrt{S^2-4}}.$$

$$\frac{dW_{\mathrm{FWHM}}}{dS} = -\frac{4S\operatorname{arcosh}(\sqrt{2})}{(S^2-4)^{3/2}}.$$

The previous illustrative interval has therefore been removed because it crossed the zero-discriminant boundary. The revised illustration remains on a single admissible branch:

$$2.1 \leq S \leq 3.5, \qquad T = 1.$$

Figures 1 and 2 illustrate the two nondegenerate NIC phase-plane configurations. The saddle and center exchange when the sign of the discriminant changes. The closed curves near the center are interpreted as regular

level sets of the first integral rather than being inferred from the Jacobian alone. In Figure 3, the red curve represents the soliton width, which decreases as (S) increases, whereas the blue curve represents the soliton amplitude, which gradually increases with (S).

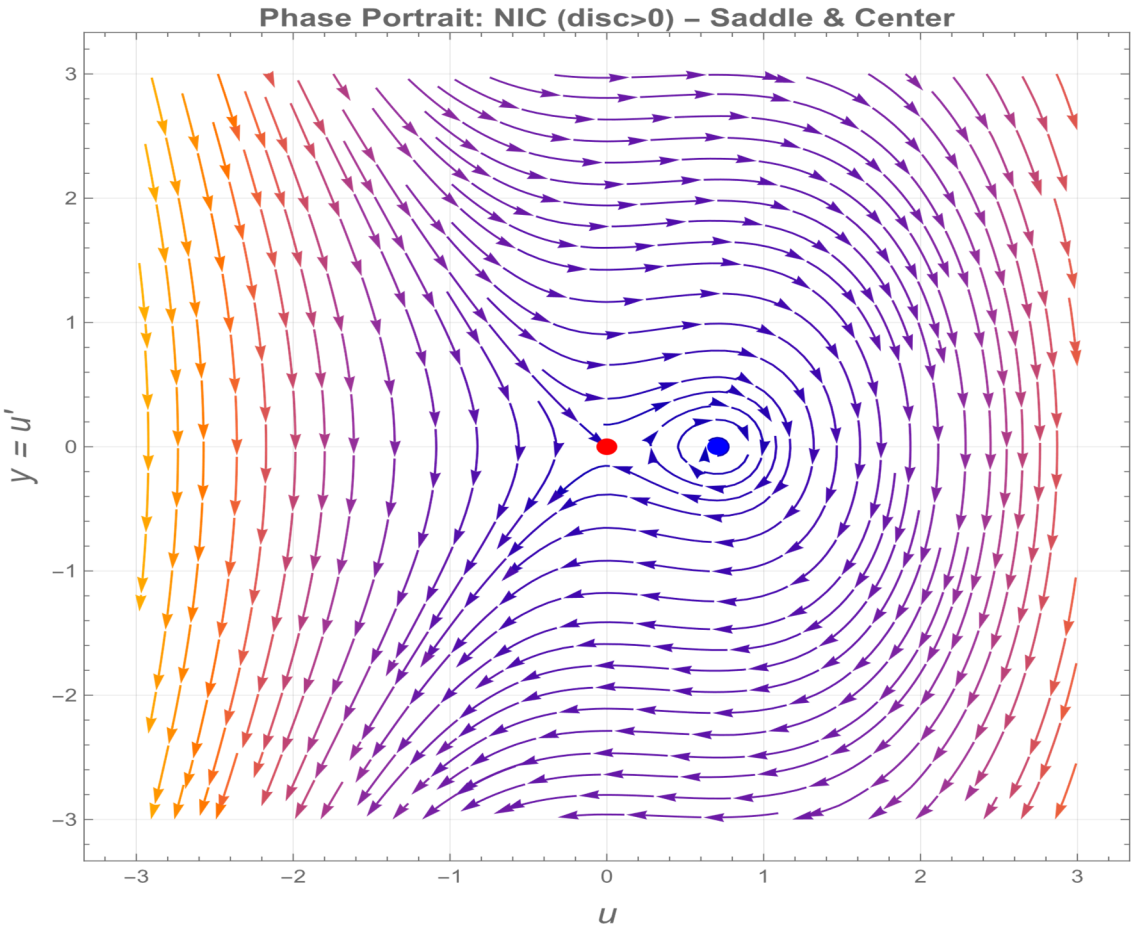


Figure 1. Phase portrait of the planar dynamical system for the NIC model. when $D > 0$ $(S = \sqrt{5}, T = 1)$.

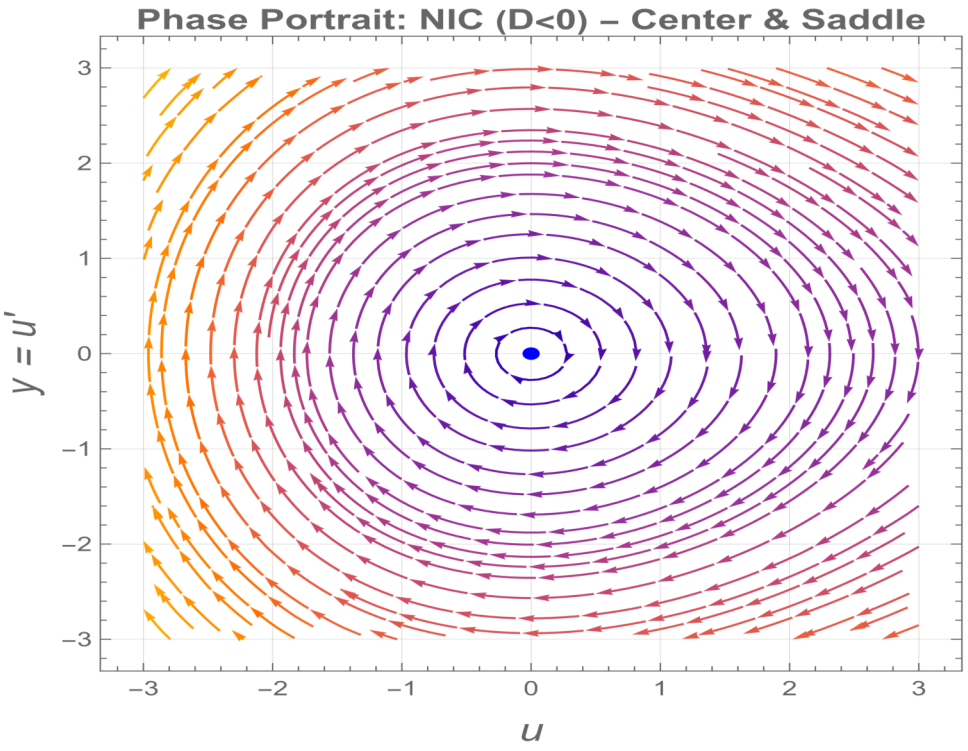


Figure 2. Phase portrait for the NIC model when $\mathrm{D} < 0$ $(\mathrm{S} = \sqrt{3}, \mathrm{T} = 1)$.

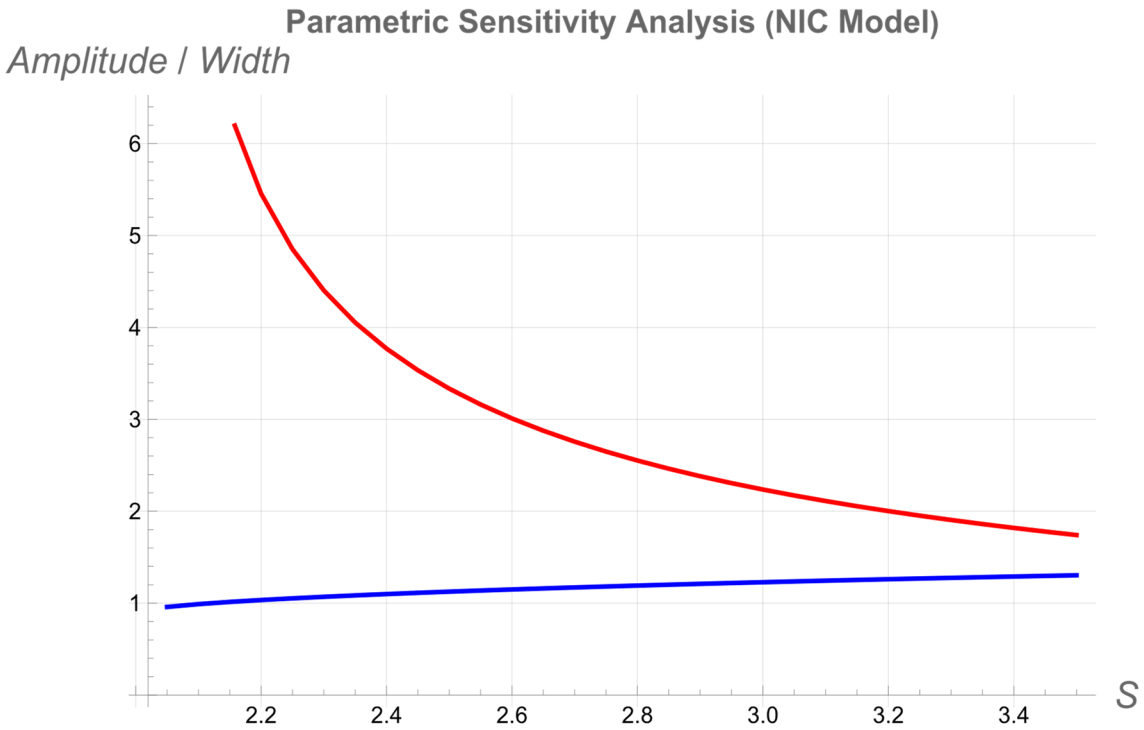


Figure 3. Parametric sensitivity of the soliton characteristics with respect to the bifurcation parameter S.

The verified CSK Set-1 pulse satisfies the restricted Hamiltonian relation stated in Section 5.2. This is not an identification of the complete CSK system with the NIC model, and no D-dependent topology is asserted for the entire fifth-order equation.

Admissibility and regularity conditions. In addition to the branch conditions, every algebraic denominator must remain nonzero. The principal restrictions and sufficient non-vanishing conditions are

$$T \neq 0, \qquad a_0 \neq 0, \qquad k = S - T - 1 \neq 0.$$

$$S^2 + 2T - 6ST + 6T^2 \neq 0.$$

$$Q_+(\delta) = C_1 + C_2 e^{\sqrt{D}\,\delta}.$$

$$C_1 C_2 \geq 0, \qquad (C_1, C_2) \neq (0,0).$$

$$Q_-(\delta) = C + B\sin\theta + E\cos\theta.$$

$$|C| > \sqrt{B^2 + E^2}.$$

$$R_{\mathrm{NIC}} = u'' - \frac{\beta\varepsilon}{2}u^2 + (6 - \gamma\varepsilon)u.$$

$$TR_{\mathrm{NIC}} \equiv 0.$$

$$R_{\mathrm{CSK}} = -cv' + 45v^2v' + 15v'v'' + 15vv''' + v^{(5)}.$$

$$R_{\mathrm{CSK}} \equiv 0.$$

6. Analysis of 3D, 2D, and Contour Profiles

The graphical representation and analysis section of this paper provides a comprehensive visual exploration of the NIC equation and its relationship to the CSK equation. This section aims to elucidate the complex dynamics and behaviors exhibited by these equations through a series of carefully constructed figures and analytical representations. The following graphical elements and accompanying analyses serve to illuminate key aspects of our research, including phase space trajectories, solution profiles, and comparative studies of the NIC and CSK equations. These visual aids not only support our theoretical findings but also provide an intuitive understanding of the underlying physical processes, facilitating a broader comprehension of nano-ionic currents and their potential applications in various scientific and technological domains. To illustrate our findings using specific parameter values, we have generated graphical representations of the explicit solutions derived in Equations' (12), (14), (18), and (27) for the proposed equations. The solutions are illustrated in Figures 4–7, displaying them in 3D and 2D formats, as well as contour patterns. The obtained shapes depict the bell-shaped soliton, compacton-shaped soliton, flat kink-shaped soliton, and smooth kink-shaped soliton.

We note that the remaining analytical solutions, obtained from different parameter sets, exhibit spatial profiles that are qualitatively identical to the presented profiles in Figures 4–7 and they simply correspond to same amplitudes, widths, or asymptotic tails, and since no new topological class or distinct physical structure emerges from those variants, we have intentionally omitted their 3D, 2D, and contour plots to preserve the conciseness and focus of this manuscript. The selected figures capture the all-essential bifurcation regimes and representative wave patterns.

In Figure 4, the selected parameters satisfy the positive-discriminant condition

$$D = S^2 - 4T > 0.$$

Therefore, the plotted solution belongs to the positive-discriminant branch. The bell-type profile is identified from the analytical solution by its localized excursion and equal finite asymptotic limits, rather than from the phase portrait alone.

In Figure 5, Equation (14) is plotted with $S = 0, T = 1, A_1 = 1, A_2 = 0, a_0 = 1, D = -4, \omega = 1$, and $\delta = x - 0.1t$ on $-0.4 \le x \le 0.4$ and $0 \le t \le 0.4$. In this rectangle, $-0.44 \le \delta \le 0.4$, and the denominator $2(sin\ \delta - cos\ \delta)$ never vanishes: its absolute value is at least $2(cos\ 0.4 - sin\ 0.4) > 1.06$. The branch is regular only on the displayed interval, not globally nonsingular.

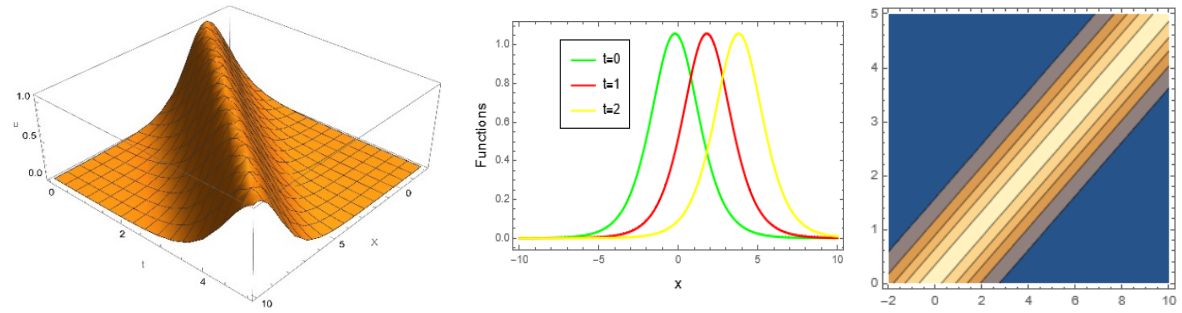


Figure 4. The bell-shaped soliton for Equation (12) with the given values, (**i**) 3D plot, (**ii**) 2D plot, and (**iii**) contour plot.

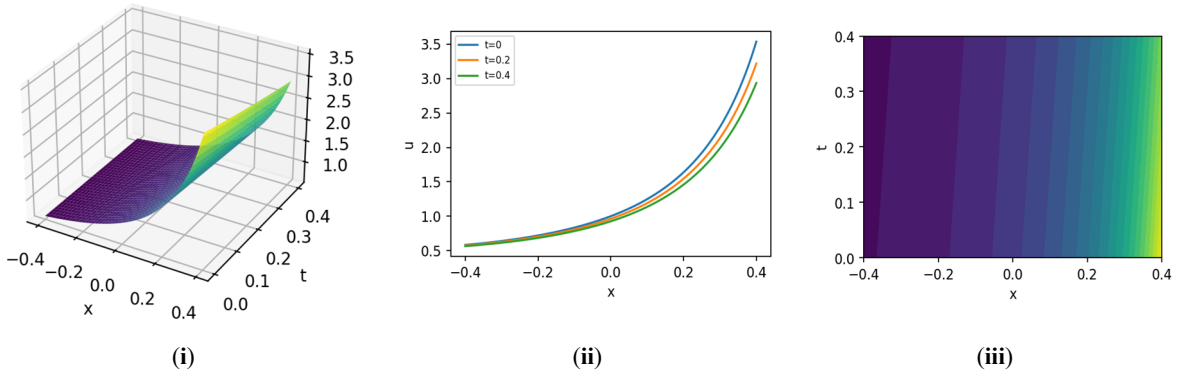
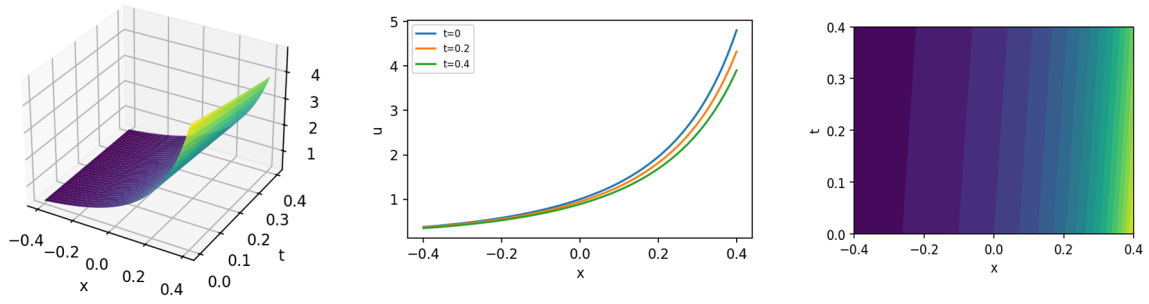


Figure 5. Regular finite-domain trigonometric profile from Equation (14), with $S = 0, T = 1, A_1 = 1, A_2 = 0, a_0 = 1, \delta = x - 0.1t, -0.4 \le x \le 0.4\ and\ 0 \le t \le 0.4$; (**i**) 3D, (**ii**) 2D and (**iii**) contour.

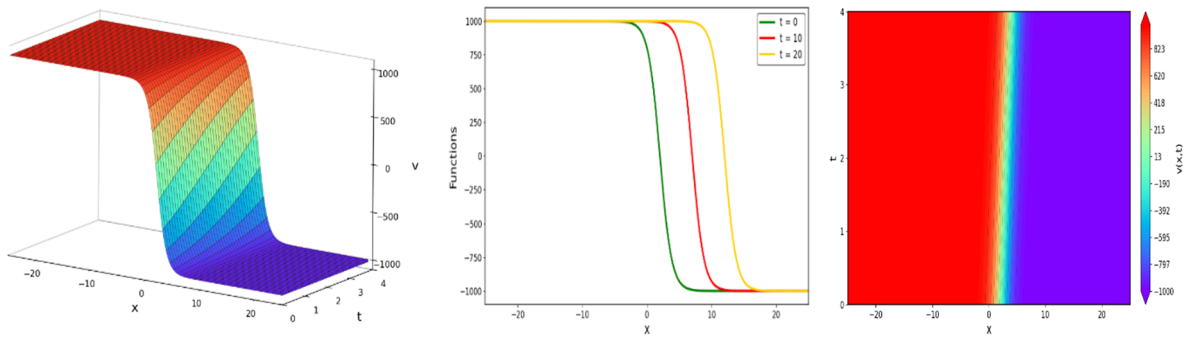
In Figure 6, Equation (18) is plotted using the same parameters, traveling variable, and domain as Figure 5. The shared trigonometric denominator is again $2(sin\,\delta - cos\,\delta)$, so the identical lower bound proves the absence of poles on this domain. The profile is a regular local segment of a meromorphic trigonometric solution and is not claimed to be a globally nonsingular kink.

In Figure 7, the solution belongs to the positive-discriminant exponential branch, satisfying $D = S^2 - 4T > 0$. The wave profile is classified from its asymptotic end states. In addition, the auxiliary constants A_1 and A_2 are chosen so that the denominator of the analytical solution remains nonzero throughout the displayed domain, thereby ensuring a regular and nonsingular wave profile.



(i) **(ii)** **(iii)**

Figure 6. Regular finite-domain trigonometric profile from Equation (18), using the same parameters and domain as Figure 5; **(i)** 3D, **(ii)** 2D and **(iii)** contour.



(i) **(ii)** **(iii)**

Figure 7. The smooth kink-shaped soliton for Equation (27) with the given values, **(i)** 3D plot, **(ii)** 2D plot, and **(iii)** contour plot.

7. Comparison of the Results and Originality

When comparing the results in existing research to the solutions derived from our work on the NIC equation and the CSK equation, it's essential to break down the distinctions and advantages based on the context of application, methodology, and the behavior of the equations under different conditions. Here's a structured comparison of the results to the NIC equation in Table 2.

Table 2. Comparison of existing research and the present study on the NIC equation.

Existing Research	Our Research
Traditional models and results in nano- ionic systems in the references [52], are often focused on simplified approaches for analyzing ionic transport at nanoscale dimensions, and results in [56], rely heavily on approximations that work well under standard assumptions but can deviate in more complex real-world scenarios. Results in references [53,54], approaches often don't fully capture the intricate coupling between electrostatic forces and ionic motion within nanostructures or devices like memristors and nano-batteries.	Our results likely include more refined techniques for solving the nano-ionic currents equation, accounting for non-idealities as well as Strong ion-ion interactions in confined geometries. Our results give a nonlinear response of nano-ionic transport under varying external fields, better integration of quantum mechanical effects or surface interactions, where ionic behavior differs drastically compared to bulk, and also provide mathematical robustness.

Again, here's a structured comparison of the results to the CSKS equation in Table 3.

Table 3. Comparison of existing research and the present study on the CSK equation.

Existing Research	Our Research
Results in existing research in the references [51,57,58], are effective in classical soliton theory, but may not always accommodate modifications to the equation that arise in real-world physical contexts. Results in existing research in the reference [49], are often constrained to idealized boundary conditions or specific initial conditions.	Our results can expand upon classical methods by offering a broader class of solitons, potentially including rogue waves, breathers, or localized structures not captured in prior research, and can give advanced analytic techniques that go beyond the typical soliton solutions, thus increasing the practical relevance of the results.

All results of the NIC equation and the CSK equation include more sophisticated physical models, making them highly applicable in real-world engineering and scientific contexts. In essence, our results can stand out due to their broader generalizability, higher accuracy in modeling complex phenomena, and adaptability to various real-world conditions, which are crucial for advancing both theoretical understanding and technological applications. In addition, if our research introduces novel mathematical techniques, this can lead to deeper insights into the behavior of systems governed by these equations, making your work foundational for future developments.

8. Conclusions

In this work, exact traveling-wave families are derived for the NIC and CSK equations and then examined through dynamical-system relations associated with the expansion ansatz. For the NIC Set-1 family, a first integral rigorously supports the local nonlinear center and the surrounding closed energy levels. For the CSK equation, the restricted phase-plane analysis now follows the verified sech^2 Set-1 pulse and is not claimed to describe the full fifth-order dynamics. For the NIC model, the saddle and center exchange roles between $D > 0$ and $D < 0$, while $D = 0$ is a degenerate threshold. The sensitivity analysis is restricted to an admissible $D > 0$ branch and uses explicit amplitude/FWHM derivatives. The term “compacton” has been removed because compact support has not been established; trigonometric nonsingular branches are described as periodic/oscillatory. These revisions make the dynamical interpretation consistent with the exact solution formulas and their admissibility conditions.

Author Contributions

M.A.A.: Conceptualization, Methodology, Formal analysis, Visualization, Writing—original draft; M.A.I.: Validation, Investigation, Software, Writing—review & editing. All authors have read and agreed to the published version of the manuscript.

Funding

This research received no external funding.

Institutional Review Board Statement

Not applicable.

Informed Consent Statement

Not applicable.

Data Availability Statement

No datasets were generated or analyzed during the current study.

Conflicts of Interest

The authors declare no conflict of interest.

Use of AI and AI-Assisted Technologies

No AI tools were utilized for this paper.

References

1. El-Ganaini, S.I.A. The First Integral Method to the Nonlinear Schrodinger Equations in Higher Dimensions. *Abstr. Appl. Anal.* **2013**, *2013*, 349173. https://doi.org/10.1155/2013/349173.
2. Ahmed, N.; Bibi, S.; Khan, U.; et al. A new modification in the exponential rational function method for nonlinear fractional differential equations. *Eur. Phys. J. Plus* **2018**, *133*, 45. https://doi.org/10.1140/epjp/i2018-11896-0.
3. Chadwick, E.; Hatam, A.; Kazem, S. Exponential function method for solving nonlinear ordinary differential equations with constant coefficients on a semi-infinite domain. *Proc. Math. Sci.* **2016**, *126*, 79–97. https://doi.org/10.1007/s12044-015-0254-3.
4. Raza, N.; Osman, M.S.; Abdel-Aty, A.H.; et al. Optical solitons of space-time fractional Fokas–Lenells equation with two versatile integration architectures. *Adv. Differ. Equ.* **2020**, *2020*, 517. https://doi.org/10.1186/s13662-020-02973-7.
5. Malwe, B.H.; Betchewe, G.; Doka, S.Y.; et al. Travelling wave solutions and soliton solutions for the nonlinear transmission line using the generalized Riccati equation mapping method. *Nonlinear Dyn.* **2016**, *84*, 171–177. https://doi.org/10.1007/s11071-015-2318-4.
6. Ndiaye, M. The Riccati Equation, Differential Transform, Rational Solutions and Applications. *Appl. Math.* **2022**, *13*, 774–792. https://doi.org/10.4236/am.2022.139049.
7. Its, A.; Its, E.; Kaplunov, J. Riemann–Hilbert Approach to the Elastodynamic Equation: Part I. *Lett. Math. Phys.* **2011**, *96*, 53–83. https://doi.org/10.1007/s11005-010-0448-7.
8. Wu, J. A novel Riemann–Hilbert approach via *t*-part spectral analysis for a physically significant nonlocal integrable nonlinear Schrödinger equation. *Nonlinearity* **2023**, *36*, 2021–2037. https://doi.org/10.1088/1361-6544/acbada.
9. Shqair, M.; Alabedalhadi, M.; Al-Omari, S.; et al. Abundant Exact Travelling Wave Solutions for a Fractional Massive Thirring Model Using Extended Jacobi Elliptic Function Method. *Fractal Fract.* **2022**, *6*, 252. https://doi.org/10.3390/fractalfract6050252.
10. Liu, S.; Fu, Z.; Liu, S.; et al. Jacobi elliptic function expansion method and periodic wave solutions of nonlinear wave equations. *Phys. Lett. A* **2001**, *289*, 69–74. https://doi.org/10.1016/s0375-9601(01)00580-1.
11. Ma, W.X. Soliton solutions by means of Hirota bilinear forms. *Partial Differ. Equ. Appl. Math.* **2022**, *5*, 100220. https://doi.org/10.1016/j.padiff.2021.100220.
12. Hirota, R. Exact envelope-soliton solutions of a nonlinear wave equation. *J. Math. Phys.* **1973**, *14*, 805–809. https://doi.org/10.1063/1.1666399.
13. Jawad, A.J.M. Tan-Cot Method to Solve (2+1)-Dimensional Bogoyavlenskii System and Konopelchenko-Dubrovsky Coupled System. *Am. J. Numer. Anal.* **2013**, *1*, 32–35. https://doi.org/10.12691/ajna-1-1-5.
14. Akbulut, A.; Kaplan, M. Auxiliary equation method for time-fractional differential equations with conformable derivative. *Comput. Math. Appl.* **2018**, *75*, 876–882. https://doi.org/10.1016/j.camwa.2017.10.016.
15. Sirendaoreji. Auxiliary equation method and new solutions of Klein–Gordon equations. *Chaos Solitons Fractals* **2007**, *31*, 943–950. https://doi.org/10.1016/j.chaos.2005.10.048.
16. Jabbari, A.; Kheiri, H. New exact traveling wave solutions for the Kawahara and Modified Kawahara equations by using modified Tanh-Coth method. *Acta Univ. Apulensis* **2010**, *23*, 21–38.
17. Alharthi, M.S.; Baleanu, D.; Ali, K.K.; et al. The dynamical behavior for a famous class of evolution equations with double exponential nonlinearities. *J. Ocean Eng. Sci.* **2022**, *in press*. https://doi.org/10.1016/j.joes.2022.05.033.
18. Hossain, A.K.M.K.S.; Akbar, M.A.; Wazwaz, A.M. Closed form solutions of complex wave equations via the modified simple equation method. *Cogent Phys.* **2017**, *4*, 1312751. https://doi.org/10.1080/23311940.2017.1312751.
19. Jawad, A.J.M.; Petković, M.D.; Biswas, A. Modified simple equation method for nonlinear evolution equations. *Appl. Math. Comput.* **2010**, *217*, 869–877. https://doi.org/10.1016/j.amc.2010.06.030.
20. Akbar, M.A.; Ali, N.H.M. An ansatz for solving nonlinear partial differential equations in mathematical physics. *SpringerPlus* **2016**, *5*, 24. https://doi.org/10.1186/s40064-015-1652-9.
21. Wang, M.; Zhou, Y.; Li, Z. Application of a homogeneous balance method to exact solutions of nonlinear equations in mathematical physics. *Phys. Lett. A* **1996**, *216*, 67–75. https://doi.org/10.1016/0375-9601(96)00283-6.
22. Osman, M.S. One-soliton shaping and inelastic collision between double solitons in the fifth-order variable-coefficient Sawada–Kotera equation. *Nonlinear Dyn.* **2019**, *96*, 1491–1496. https://doi.org/10.1007/s11071-019-04866-1.
23. Osman, M.S.; Wazwaz, A.M. A general bilinear form to generate different wave structures of solitons for a (3+1)-dimensional Boiti-Leon-Manna-Pempinelli equation. *Math. Methods Appl. Sci.* **2019**, *42*, 6277–6283. https://doi.org/10.1002/mma.5721.
24. Abdou, M.A. The extended F-expansion method and its application for a class of nonlinear evolution equations. *Chaos Solitons Fractals* **2007**, *31*, 95–104. https://doi.org/10.1016/j.chaos.2005.09.030.
25. Liu, C.P.; Chen, J.K.; Fan, C. A Direct Algebraic Method in Finding Particular Solutions to Some Nonlinear Evolution Equations. *Commun. Theor. Phys.* **2004**, *42*, 74–78. https://doi.org/10.1088/0253-6102/42/1/74.

26. Taghizadeh, N.; Mirzazadeh, M.N. The direct algebraic method for the (3+1)-dimensional Kadomtsev-Petviashvili (KP) equation. *Int. J. Appl. Math. Comput.* **2011**, *3*, 189–192.
27. Zhang, R.F.; Li, M.C. Bilinear residual network method for solving the exactly explicit solutions of nonlinear evolution equations. *Nonlinear Dyn.* **2022**, *108*, 521–531. https://doi.org/10.1007/s11071-022-07207-x.
28. Rahman, M.M.; Habib, M.A.; Shahadat Ali, H.M.; et al. The Generalized Kudryashov Method: a Renewed Mechanism for Performing Exact Solitary Wave Solutions of Some NLEEs. *J. Mech. Contin. Math. Sci.* **2019**, *14*, 323–339. https://doi.org/10.26782/jmcms.2019.02.00022.
29. Kumar, D.; Park, C.; Tamanna, N.; et al. Dynamics of two-mode Sawada-Kotera equation: Mathematical and graphical analysis of its dual-wave solutions. *Results Phys.* **2020**, *19*, 103581. https://doi.org/10.1016/j.rinp.2020.103581.
30. Abdel-Gawad, H.I.; Osman, M. On shallow water waves in a medium with time-dependent dispersion and nonlinearity coefficients. *J. Adv. Res.* **2015**, *6*, 593–599. https://doi.org/10.1016/j.jare.2014.02.004.
31. Osman, M.S.; Abdel-Gawad, H.I. Multi-wave solutions of the (2+1)-dimensional Nizhnik-Novikov-Veselov equations with variable coefficients. *Eur. Phys. J. Plus* **2015**, *130*, 215. https://doi.org/10.1140/epjp/i2015-15215-1.
32. Zhang, R.F.; Bilige, S. Bilinear neural network method to obtain the exact analytical solutions of nonlinear partial differential equations and its application to p-gBKP equation. *Nonlinear Dyn.* **2019**, *95*, 3041–3048. https://doi.org/10.1007/s11071-018-04739-z.
33. Zhang, R.F.; Li, M.C.; Yin, H.M. Rogue wave solutions and the bright and dark solitons of the (3+1)-dimensional Jimbo–Miwa equation. *Nonlinear Dyn.* **2021**, *103*, 1071–1079. https://doi.org/10.1007/s11071-020-06112-5.
34. Zhang, R.; Bilige, S.; Chaolu, T. Fractal Solitons, Arbitrary Function Solutions, Exact Periodic Wave and Breathers for a Nonlinear Partial Differential Equation by Using Bilinear Neural Network Method. *J. Syst. Sci. Complex.* **2021**, *34*, 122–139. https://doi.org/10.1007/s11424-020-9392-5.
35. Vakhnenko, V.O.; Parkes, E.J.; Morrison, A.J. A Bäcklund transformation and the inverse scattering transform method for the generalised Vakhnenko equation. *Chaos Solitons Fractals* **2003**, *17*, 683–692. https://doi.org/10.1016/s0960-0779(02)00483-6.
36. Gorguis, A. A comparison between Cole–Hopf transformation and the decomposition method for solving Burgers' equations. *Appl. Math. Comput.* **2006**, *173*, 126–136. https://doi.org/10.1016/j.amc.2005.02.045.
37. Wang, M.; Zhang, J.; Li, E.; et al. The generalized Cole–Hopf transformation to a general variable coefficient Burgers equation with linear damping term. *Appl. Math. Lett.* **2020**, *105*, 106299. https://doi.org/10.1016/j.aml.2020.106299.
38. Li, L.X.; Li, E.Q.; Wang, M.L. The (G'/G,1/G)-expansion method and its application to travelling wave solutions of the Zakharov equations. *Appl. Math. J. Chin. Univ.* **2010**, *25*, 454–462. https://doi.org/10.1007/s11766-010-2128-x.
39. Iqbal, M.A.; Wang, Y.; Miah, M.M.; et al. Study on Date–Jimbo–Kashiwara–Miwa Equation with Conformable Derivative Dependent on Time Parameter to Find the Exact Dynamic Wave Solutions. *Fractal Fract.* **2022**, *6*, 4. https://doi.org/10.3390/fractalfract6010004.
40. Sirisubtawee, S.; Koonprasert, S.; Sungnul, S. Some Applications of the (G'/G,1/G)-Expansion Method for Finding Exact Traveling Wave Solutions of Nonlinear Fractional Evolution Equations. *Symmetry* **2019**, *11*, 952. https://doi.org/10.3390/sym11080952.
41. Kara, S.; Ünsal, Ö. Analytical solutions to new forms of two nonlinear partial differential equations via two variable expansion method. *Partial Differ. Equ. Appl. Math.* **2022**, *5*, 100210. https://doi.org/10.1016/j.padiff.2021.100210.
42. Zhang, Z.; Wu, J. Generalized-expansion method and exact traveling wave solutions of the perturbed nonlinear Schrödinger's equation with Kerr law nonlinearity in optical fiber materials. *Opt. Quantum Electron.* **2017**, *49*, 52. https://doi.org/10.1007/s11082-016-0884-4.
43. Ganie, A.H.; Sadek, L.H.; Tharwat, M.M.; et al. New investigation of the analytical behaviors for some nonlinear PDEs in mathematical physics and modern engineering. *Partial Differ. Equ. Appl. Math.* **2024**, *9*, 100608. https://doi.org/10.1016/j.padiff.2023.100608.
44. Iqbal, M.A.; Miah, M.M.; Rasid, M.M.; et al. An investigation of two integro-differential KP hierarchy equations to find out closed form solitons in mathematical physics. *Arab. J. Basic Appl. Sci.* **2023**, *30*, 535–545. https://doi.org/10.1080/25765299.2023.2256049.
45. Mia, R.; Miah, M.M.; Osman, M.S. A new implementation of a novel analytical method for finding the analytical solutions of the (2+1)-dimensional KP-BBM equation. *Heliyon* **2023**, *9*, e15690. https://doi.org/10.1016/j.heliyon.2023.e15690.
46. Aziz, M.A.; Iqbal, M.A.; Akbar, M.A. Exploring soliton and soliton-type solutions to the modified Camassa-Holm and Schrödinger-Hirota equations: An analytical approach. *Phys. Scr.* **2025**, *100*, 025234. https://doi.org/10.1088/1402-4896/adae3f.
47. Aziz, M.A. Advanced Mathematical Approaches for the Kadomtsev–Petviashvili and Bogoyavlensky–Konopelchenko Equations in Applied Sciences. *Abstr. Appl. Anal.* **2025**, *2025*, 6164719. https://doi.org/10.1155/aaa/6164719.
48. Guo, Y.; Li, D.; Wang, J. The new exact solutions of the Fifth-Order Sawada–Kotera equation using three wave method. *Appl. Math. Lett.* **2019**, *94*, 232–237. https://doi.org/10.1016/j.aml.2019.03.001.

49. Riaz, M.B.; Naseer, F.; Abbas, M.; et al. Solitary wave solutions of Sawada-Kotera equation using two efficient analytical methods. *AIMS Math.* **2023**, *8*, 31268–31292. https://doi.org/10.3934/math.20231601.
50. Gardner, C.S.; Greene, J.M.; Kruskal, M.D.; et al. Method for Solving the Korteweg-deVries Equation. *Phys. Rev. Lett.* **1967**, *19*, 1095–1097. https://doi.org/10.1103/physrevlett.19.1095.
51. Sawada, K.; Kotera, T. A Method for Finding N-Soliton Solutions of the K.d.V. Equation and K.d.V.-Like Equation. *Prog. Theor. Phys.* **1974**, *51*, 1355–1367. https://doi.org/10.1143/ptp.51.1355.
52. Islam, S.M.R. Bifurcation analysis and exact wave solutions of the nano-ionic currents equation: Via two analytical techniques. *Results Phys.* **2024**, *58*, 107536. https://doi.org/10.1016/j.rinp.2024.107536.
53. Choy, K.L.; Su, B. Growth behavior and microstructure of CdS thin films deposited by an electrostatic spray assisted vapor deposition (ESAVD) process. *Thin Solid Films* **2001**, *388*, 9–14. https://doi.org/10.1016/s0040-6090(00)01894-0.
54. Boiarska, Z.; Passarella, D. Microtubule-targeting agents and neurodegeneration. *Drug Discov. Today* **2021**, *26*, 604–615. https://doi.org/10.1016/j.drudis.2020.11.033.
55. Mitchison, T.; Kirschner, M. Dynamic instability of microtubule growth. *Nature* **1984**, *312*, 237–242. https://doi.org/10.1038/312237a0.
56. Satarić, M.V.; Sekulić, D.; Živanov, M. Solitonic Ionic Currents Along Microtubules. *J. Comput. Theor. Nanosci.* **2010**, *7*, 2281–2290. https://doi.org/10.1166/jctn.2010.1609.
57. Hirota, R. *The Direct Method in Soliton Theory*; Cambridge University Press: Cambridge, UK, 2004. https://doi.org/10.1017/cbo9780511543043.
58. Akhmediev, N.; Ankiewicz, A. *Solitons: Non-linear Pulses and Beams*; Springer: New York, NY, USA, 1997.